

Synthesis and photophysics of porphyrin–fullerene donor–acceptor dyads with conformationally flexible linkers

David I. Schuster,^{a,*} Shaun MacMahon,^a Dirk M. Guldi,^b Luis Echegoyen^c
and Silvia E. Braslavsky^d

^aDepartment of Chemistry, New York University, New York, NY 10003, USA

^bInstitute for Physical and Theoretical Chemistry, University of Erlangen, 91058 Erlangen, Germany

^cDepartment of Chemistry, Clemson University, Clemson, SC 29634, USA

^dMax Planck Institute for Bioinorganic Chemistry (formerly Strahlenchemie), D 45413 Mülheim, Germany

Received 7 June 2005; revised 26 July 2005; accepted 30 July 2005

Available online 15 December 2005

Abstract—The synthesis and photophysics of a series of porphyrin–fullerene (P–C₆₀) dyads in which the two chromophores are linked by conformationally flexible polyether chains is reported. Molecular modeling indicates the two moieties adopt a stacked conformation in which the two chromophores are in close proximity. Photoexcitation of the free base dyads in polar solvents such as tetrahydrofuran and benzonitrile, causes electron transfer (ET) to generate charge-separated radical pair (CSRP) states, which were directly detected using transient absorption (TA) techniques. In nonpolar solvents such as toluene, where CSRP states were not directly detected, fullerene triplet state states were formed, according to TA studies as well as singlet oxygen sensitization measurements. The low value of the quantum efficiency for sensitized formation of singlet molecular oxygen [O₂(¹Δ_g)] in toluene and chloroform indicates that singlet energy transduction to give H₂P–¹C₆₀*, followed by intersystem crossing to H₂P–³C₆₀* and energy transfer to ³O₂, is not the operative mechanism. Rather, a mechanism is proposed involving ET to give CSRP states followed by exergonic charge recombination to eventually generate fullerene triplets. Such a mechanism has been demonstrated experimentally for structurally related P–C₆₀ dyads. For the corresponding ZnP–C₆₀ dyads with flexible linkers, only photoinduced ET to generate long-lived CSRP states is observed. Photoinduced charge separation in these dyad systems is extremely rapid, consistent with a through space rather than through-bond mechanism. Charge recombination is up to three orders of magnitude slower, indicating this process occurs in the inverted region of the Marcus curve that relates ET rates to the thermodynamic driving force. These observations once again demonstrate the advantages of incorporating fullerenes as electron acceptor components in photosynthetic model systems.

© 2005 Elsevier Ltd. All rights reserved.

1. Introduction

Fullerenes, C₆₀ in particular, have been found to make ideal acceptors in model photosynthetic systems, due to their unique photophysical, electrochemical, and chemical properties.¹ C₆₀ has been shown to reversibly accept up to six electrons in solution due to its three low lying degenerate lowest unoccupied molecular orbitals (LUMOs), with a first electrode potential resembling that of the quinone-derived electron acceptor in the photosynthetic reaction center.² Fullerenes accelerate charge separation and slow down charge recombination versus donor–acceptor (DA) dyads containing traditional two-dimensional electron acceptors such as quinones and imides. This phenomenon, which is general, has been rationalized by the small Marcus

reorganization energy (λ) accompanying electron transfer in fullerenes. Since the negative charge on the fullerene produced after photoexcitation of the donor moiety is delocalized over the entire π -system, the charge density is much lower than it would be on acceptors such as quinones, where the charge is concentrated mainly on the oxygens. The structural inflexibility of fullerene-based systems results in small internal reorganization energies (λ_v), while the charge dispersion minimizes the solvent reorganization energy (λ_s).³

For electron DA systems, Marcus theory predicts that as the free energy change (ΔG^0) for electron transfer (ET) becomes more negative, that is, increasingly exergonic, the ET rates increase, reaching a maximum when $-\Delta G_{ET} = \lambda$, the reorganization energy. As $-\Delta G_{ET}^0$ becomes more negative than the absolute value of λ , the ET rate decreases. For C₆₀ dyads, the maximum in the Marcus curve is reached at smaller values of $-\Delta G_{ET}^0$ compared to two-dimensional acceptors.

Keywords: Fullerenes; Porphyrins; Dyads.

* Corresponding author. Tel.: +1 212 998 8447; fax: +1 212 260 7905; e-mail: david.schuster@nyu.edu

Thus, charge separation (CS) rates for most fullerene-based DA dyads are located along the upward slope of the Marcus curve, near the maximum, leading to enhanced CS rates, whereas the large thermodynamic driving force for charge recombination (CR) places this process on the downward side of the Marcus parabola in the inverted region. This phenomenon causes a noticeable enhancement in the lifetime of charge-separated radical pair (CSRP) states in C₆₀-based DA systems versus analogous two-dimensional DA systems.⁴

Porphyrins are frequently used as donors in artificial photosynthetic systems. Porphyrins are synthetically accessible in a laboratory, (although their synthesis can be a rather arduous task),⁵ and they absorb light much more effectively than fullerenes in the visible region between 400 and 600 nm. Favorable van der Waals interactions between the curved π surface of the fullerene and the planar π surface of the porphyrin assist in the formation of supramolecular structures, overcoming the necessity to match a concave-shaped host to a convex-shaped guest.⁶ This unique intermolecular electronic interaction is observed in condensed media as well as in the solid state.

Attempts to suppress CR have led to the development of multi-chromophoric triads, tetrads and pentads, where ET can occur through a multi-step process, yielding CSRP with microsecond to second lifetimes.^{1c,d,7} An inherent problem is the synthetic challenge involved in the synthesis of such complicated assemblies. These multicomponent materials are far less efficient in the storage of energy than dyad systems, since sequential ET dissipates more and more of the initial excitation energy, lowering the capacity for energy storage.

Herein, we report on simple porphyrin–C₆₀ (P–C₆₀) dyads with flexible linkers, which are easily synthesized and which have many of the desirable properties of DA systems with respect to energy storage and CSRP state lifetimes.

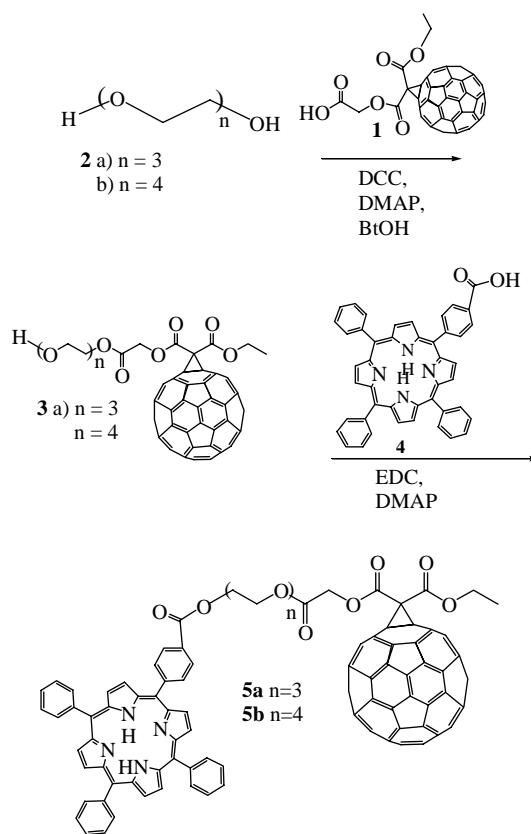
2. Free base porphyrin–fullerene dyads (H₂P–C₆₀)

2.1. Synthesis and structural characterization

Our initial foray into this area centered on the synthesis of porphyrin–fullerene (H₂P–C₆₀) dyads with flexible crown ether-like glycol linkers by a convergent route.⁸ Steady-state fluorescence spectra demonstrated rapid and efficient quenching of the porphyrin S₁ state by the fullerene, but the CS and CR kinetics were not measured on these phase I dyads. Among the synthetic problems encountered were the extremely low yields (i.e., ~30%) when using simple methanofullerene carboxylic acid, due to the acid poor solubility properties. Coupling of tetraphenylporphyrin carboxylic acid to the polyether linker also proved difficult, making it extremely challenging to generate dyads on a milligram scale.

In order to circumvent these problems, fullerene carboxylic acid **1**, originally reported by Diederich and Nierengarten,⁹ was used as the fullerene synthon. The strategy was to replace methanofullerene carboxylic acid by **1**, which would lead to flexibly linked H₂P–C₆₀ dyads with much better

solubility properties, as well as higher yields in the coupling reactions. Improved solubility would in turn allow more facile structural characterization. In the first series of reactions, summarized in Scheme 1, fullerene acid **1** was condensed with glycols **2a** and **2b** to give **3a** and **3b**, respectively, which were then condensed with 5,10,15,20-tetraphenylporphyrin carboxylic acid **4** to give dyads **5a** and **5b**, respectively. Details of these reactions are provided in an earlier paper dealing with the synthesis of a variety of P–C₆₀ dyads.¹⁰



Scheme 1.

¹H NMR spectra of **5a** and **5b** showed characteristic porphyrin bands between 7.5 and 9 ppm, glycol bands at 3.5–4 ppm, and distinctive peaks from the C₆₀ synthon **1**. Computer modeling using Insight II provided a prediction of the H₂P–C₆₀ geometry in the ground state (see Fig. 1).¹¹ Because of favorable porphyrin–fullerene π – π interactions, the glycol linker curves around, placing the porphyrin and fullerene within van der Waals contact range.

UV–vis spectra of dyads **5a** and **5b** in chloroform demonstrated strong ground state interactions. The porphyrin Soret bands at 422 nm were red shifted by approximately 5–10 nm relative to methyl ester **8**, indicating that the fullerene was close enough to the porphyrin in the ground state to perturb its absorption spectrum. Similar spectral shifts were also visible in the porphyrin Q-band region in both dyads. The broadness of the absorption in both the Soret and Q-band regions was surprising, and could indicate the presence of more than one conformation of these dyads in solution.

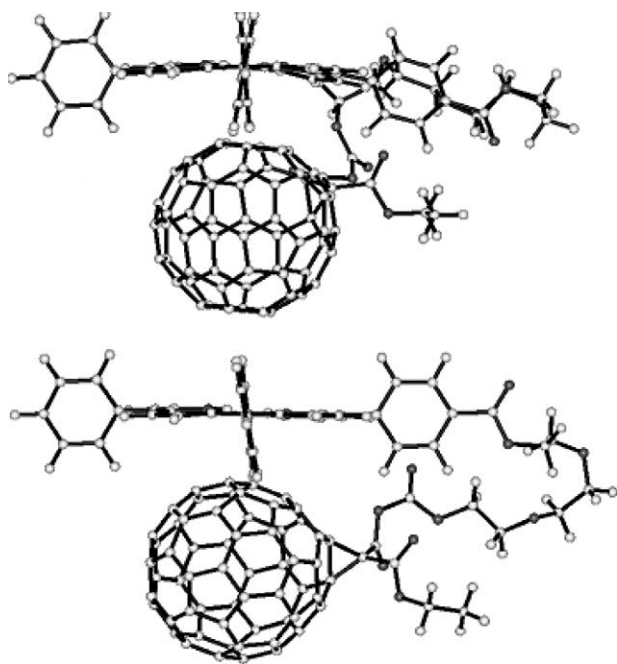


Figure 1. Insight II molecular mechanics calculations for dyads **5a** and **5b**.

Whereas substantial improvements in yield were observed in the coupling yields using fullerene carboxylic acid **1**, the porphyrin coupling step still proved to be extremely difficult. Moreover, the solubility of dyads **5a** and **5b**, though somewhat improved over the first generation dyads, still severely restricted the choice of solvents for photophysical studies. In order to improve the solubility characteristics of the porphyrin component, *tert*-butyl substituents were incorporated on the benzene rings, as in a large body of work in this field. The stepwise synthetic route to the solubilized porphyrin carboxylic acid **6** shown in Scheme 2 was developed. The first step involved preparation of a dipyrromethane derivative **7** from pyrrole and 3,5-di-*t*-butyl benzaldehyde, followed by condensation with 1 equiv each of this aldehyde and

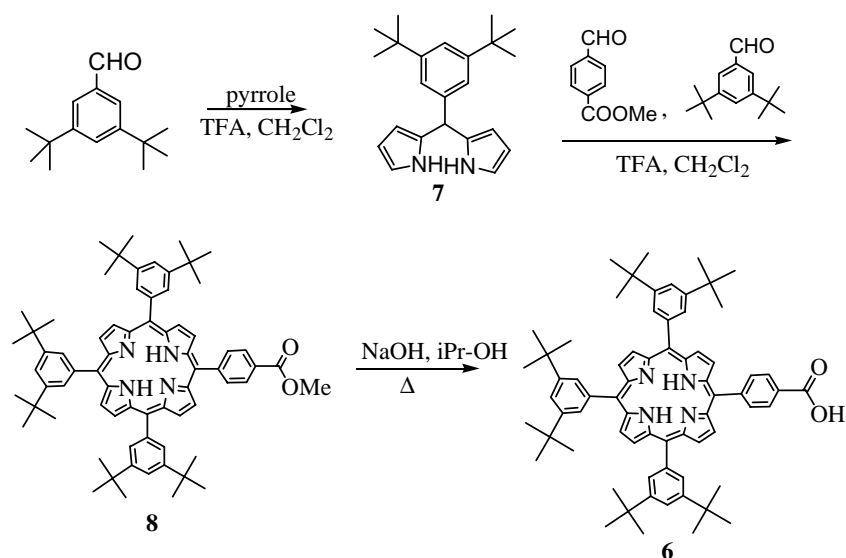
4-carboxymethylbenzaldehyde to give porphyrin methyl ester **8**. Overall yields of purified porphyrin were 17%. Hydrolysis gave carboxylic acid **6** in 94% yield.

Scheme 3 depicts the synthesis of the solubilized flexibly linked H₂P–C₆₀ dyads. The initial coupling reaction to fullerene acid **1** was carried out as before. Coupling of **3a** and **3b** to the porphyrin acid **6** using 1-(3-dimethylamino-propyl)-3-ethylcarbodiimide/dimethyl-aminopyridine (EDC/DMAP) gave the desired dyads **9a** and **9b** in 50% yield.

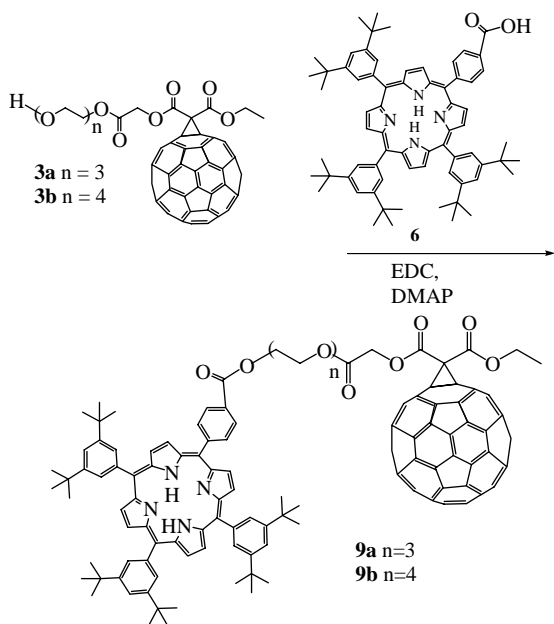
Intramolecular electronic interactions were again monitored using UV–vis spectroscopy. Bathochromic shifts of the porphyrin Soret band were pronounced, ranging from 6–10 nm depending on the solvent. The UV–vis spectra for dyads **9a** and **9b** were collected in solvents of greatly varying relative permittivity: toluene (2.0), THF (7.6), CH₂Cl₂ (9.1), and benzonitrile (PhCN) (26.0). An increase in the porphyrin–fullerene interaction was seen with increasing solvent polarity, particularly in **9b**. In relatively nonpolar solvents such as toluene and THF, the interaction between the chromophores in **9a** was stronger than in **9b**, according to shifts in the Soret band. As the solvent became more polar, the interaction in **9b** became comparable to that in **9a**. This may be because the chromophores are not as effectively solvated in polar media. It is remarkable that the interaction persists even in toluene, possibly because both the porphyrin and fullerene moieties are effectively solvated in aromatic solvents, and therefore must overcome a large entropic barrier to interact with each other. Such effects should be more pronounced with **9a** and **9b** versus **5a** and **5b** due to the presence of three di-*tert*-butylphenyl groups.

2.2. Electrochemistry

For **9a**, the first reductive redox couple of the C₆₀ center appears at –0.55 V versus Ag/AgCl, which is in good agreement with values typically observed for C₆₀ derivatives.¹² The first one-electron oxidation of the porphyrin



Scheme 2.



Scheme 3.

center occurs at +1.10 V, which is a bit more positive than that for tetraphenylporphyrins (typically +1.0 V). The small shifts are attributable to the intramolecular interactions in the dyad. Dyad **9b** showed a weak wave for the oxidation of the porphyrin center at 1.08 V, but no discernible peak for the reduction of the C₆₀ moiety was observed, probably due to the small amount of sample available. Similar measurements were not performed on **5a** and **5b**.

2.3. Steady-state fluorescence

The steady-state fluorescence properties of the flexibly linked H₂P–C₆₀ dyads were measured against that of a porphyrin standard, namely the methyl ester **8**, which has a fluorescence lifetime of 9 ns. Strong quenching in dyads **5a** and **5b** was seen relative to the standard in both benzene (Fig. 2) and chloroform (Fig. 3). To avoid signal saturation due to excessive absorption of the incident excitation light, the excitation was carried out at 550 nm, a region well separated from the Soret peak where the light is still absorbed exclusively by the porphyrin moiety. The other option available was to use extremely dilute solutions with

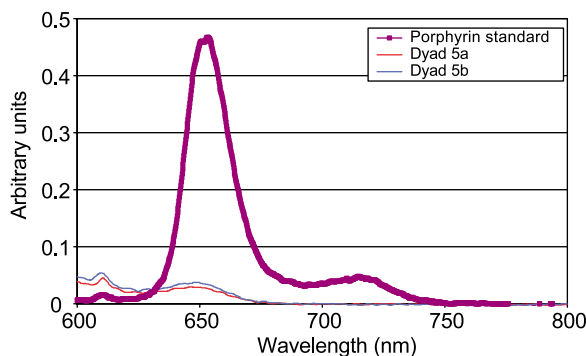


Figure 2. Fluorescence emission for dyads **5a** and **5b** in benzene (10 μ M). The porphyrin standard was methyl ester **8**.

excitation in the Soret band to the porphyrin S₂ state. The rate constant for fluorescence deactivation was higher in chloroform, which we ascribe to the increased rate of electron transfer quenching expected in the more polar solvent (*vide infra*). An increase in fluorescence quenching as a function of increasing solvent relative permittivity was observed. The quenching efficiency for dyads **5a** and **5b** both increase upon going from *o*-dichlorobenzene (ODCB) to PhCN to *N,N*-dimethylformamide (DMF).

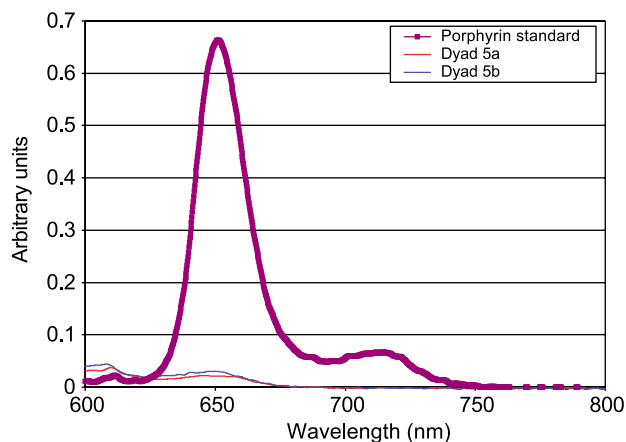


Figure 3. Fluorescence emission for dyads **5a** and **5b** in CHCl₃ (10 μ M). The porphyrin standard was methyl ester **8**.

The fluorescence properties of **9a** and **9b** were measured against that of the methyl ester of **6** as the porphyrin standard, with a fluorescence lifetime of 9 ns. Again, rapid and efficient quenching of porphyrin fluorescence in **9a** and **9b** was observed. The rate and efficiency of fluorescence quenching increased with increasing solvent polarity, as was seen with **5a** and **5b**.

2.4. Quantum yields for singlet oxygen formation

Quantum yields of sensitized singlet oxygen [O₂(¹ Δ_g)] formation (Φ_Δ) by dyads **5a** and **5b** upon excitation of air-saturated solutions at 532 nm are shown in Table 1. Full details of the procedure are given elsewhere.¹³ Quantum yields are reported relative to tetraphenylporphine (TPP) for which $\Phi_\Delta = 0.67 \pm 0.14$.¹⁴ The Φ_Δ value is an indirect way to measure ³C₆₀ formation, since ³C₆₀ transfer energy to ³O₂ to generate O₂(¹ Δ_g) occurs with unit efficiency, and for simple fullerene derivatives Φ_Δ is generally > 0.9.¹⁵ The Φ_Δ values for **5a** and **5b** are lower in chloroform than in toluene, where the values are the same for both dyads. The low Φ_Δ value in toluene indicates that singlet energy transduction to give H₂P–¹C₆₀^{*}, followed by intersystem crossing to H₂P–³C₆₀^{*} and energy transfer to ³O₂, is not operative.

Table 1. Quantum yields for O₂(¹ Δ_g) formation

| Compound | Φ (relative) in PhMe | Φ (relative) in CHCl ₃ |
|--------------------------|---------------------------|--|
| Porphyrin standard (TPP) | 0.89 | 0.94 |
| Dyad 5a | 0.34 | 0.18 |
| Dyad 5b | 0.34 | 0.09 |

Excitation of air-saturated solutions at 532 nm. For procedural details, see Ref. 13.

If such a mechanism were operative, the values of Φ_{Δ} should have been much higher, in the range 0.9–1.0.¹⁵ Such a sequence has indeed been proposed for some H₂P–C₆₀ dyads in nonpolar solvents.^{16,17} However, another possible mechanism involves electron transfer in nonpolar solvents followed by back electron transfer to generate lower lying porphyrin and fullerene triplet states. Indeed, recent time-resolved electron paramagnetic resonance (TREPR) studies have established¹⁸ that the following stepwise mechanism is operative for a parachute-shaped ZnP–C₆₀ dyad system in toluene: (1) electron transfer to give a charge-separated state, (2) back electron transfer to give ³ZnP*–C₆₀, and finally (3) energy transfer to give the lower lying ZnP–³C₆₀*. Although we have no TREPR data as yet on dyads **5a** and **5b**, we propose that a similar mechanism is operative in the present case. It is interesting to note that the triethylene glycol-linked dyad **5a** generates twice as much O₂(¹Δ_g) as the tetraethylene glycol-linked compound **5b** in chloroform, which would be difficult to explain if the energy transduction pathway was operative, but makes sense in terms of a stepwise mechanism for O₂(¹Δ_g) formation where three distinct steps of variable efficiency are involved. Unfortunately, because of lack of material, similar studies were not done with dyads **9a** and **9b**.

In this context, it is worth noting that generation of fullerene triplets in high yield by an electron transfer/charge recombination pathway has also been reported by Armaroli et al. for a quite different type of dyad, namely one in which C₆₀ is covalently linked to a bipyridine (bipy) moiety complexed with Ru(II).¹⁹ Excitation of the metal complex moiety gives the lowest triplet metal-to-ligand-charge-transfer (MLCT) excited state, which is quenched by electron transfer (ET) to give the C₆₀ radical anion in quantitative yield. This is followed by charge recombination to generate ³C₆₀*, again in quantitative yield, as determined by luminescence, as above. It was noted that triplet–triplet energy transfer (EnT) from ³MLCT* to ³C₆₀* does not compete with ET, because the EnT process is highly exergonic and is therefore located in the Marcus inverted region.¹⁹

2.5. Transient absorption measurements

Characteristic transient singlet and triplet spectra were recorded in the pico-, nano-, and microsecond time regime following 532 nm laser excitation. Typically, in our ultrafast experiments (i.e., 20 ps laser pulses) it is possible to see singlet excited states formed instantaneously, namely, with kinetics faster than $5 \times 10^{10} \text{ s}^{-1}$. A fast intersystem crossing process (i.e., $k_{isc} \sim 1.0 \times 10^8 \text{ s}^{-1}$) governs the fate of the

metastable singlet excited states in H₂P, leading to the corresponding triplet manifold, which we see with our slower experiments (i.e., 10 ns laser pulses). Characteristic absorption for C₆₀ triplets was seen at 720 nm (data not shown).¹⁹ For experimental details, see previous work from this collaborative team.¹³ Time-resolved transient absorption measurements with the free base dyads **9a** and **9b** completely corroborated the steady-state fluorescence experiments. The rate of decay of the S₁ singlet excited state of H₂P in THF and PhCN is much faster than the typical intersystem crossing rate of H₂P, using ps excitation and detection in the ps and ns range. Moreover, the differential absorption changes at the end of the fast decay bear no resemblance with any of the typical singlet/triplet excited state characteristics for H₂P or C₆₀.¹⁹ Instead, broad H₂P π-radical cation absorption in the visible²⁰ and C₆₀ π-radical anion absorption in the near-infrared²¹ are observed (see Fig. 4), which were then employed as convenient markers to quantify the CS efficiency and CR dynamics.

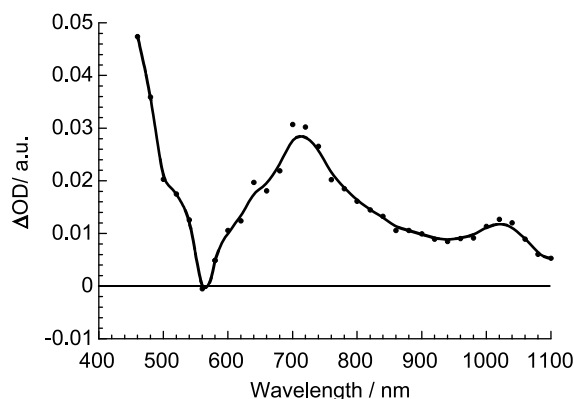


Figure 4. Differential absorption spectrum (visible and near-infrared) obtained upon nanosecond flash photolysis (532 nm) of $\sim 1.0 \times 10^{-5} \text{ M}$ solutions of **9b** in nitrogen-saturated THF with a time delay of 50 ns at room temperature. The spectrum corresponds to the radical pair H₂P^{•+}–C₆₀^{•-}.

The CS and CR dynamics in dyads **5a** and **5b**, along with the quantum yields for formation of the charge-separated states H₂P^{•+}–C₆₀^{•-} in five different solvents (Φ_{CS}), are summarized in Table 2. The lifetimes associated with CS decrease as the solvent polarity increases. Thus, the CS rates are highest in the most polar solvent, DMF, which is consistent with normal Marcus region behavior. Given that the CS rate constants vary only slightly with changes in solvent polarity, that is, they differ by less than a factor of three for both dyads, it is likely that CS in **5a** and **5b** is occurring

Table 2. Charge separation and recombination data for dyads **5a** and **5b**

| Solvent | Dyad 5a | | | Dyad 5b | | |
|---------|-------------------------------|-------------------------------|--------------------------|-------------------------------|-------------------------------|--------------------------|
| | τ_{CS} (ns) ^a | τ_{CR} (ns) ^a | Φ_{CS} ^b | τ_{CS} (ns) ^a | τ_{CR} (ns) ^a | Φ_{CS} ^b |
| Toluene | 0.188 | 373 | 0.19 | 0.222 | 396 | 0.33 |
| THF | 0.145 | 288 | 0.24 | 0.166 | 298 | 0.34 |
| ODCB | | 246 | 0.50 | | 270 | 0.67 |
| PhCN | 0.09 | 115 | 0.37 | 0.099 | 156 | 0.43 |
| DMF | 0.083 | 83 | 0.17 | 0.095 | 99 | 0.19 |

^a From formation and decay of C₆₀^{•-} absorption at 980–1020 nm.

^b From absorption at 1000 nm measured 20 ns after the flash, relative to reference dyad.

Table 3. Electron transfer dynamics for dyads **9a** and **9b**

| Compound | τ_F (ns) ^a | | τ_F (ns) ^b | | | τ_{CS} (ns) | |
|-----------|----------------------------|------|----------------------------|------|------|------------------|------|
| | THF | PhCN | PhMe | THF | PhCN | THF | PhCN |
| 8 | | | 9.6 | 9.5 | 9.8 | | |
| 9a | 0.78 | 0.74 | 1.06 | 0.95 | 0.83 | | 490 |
| 9b | 0.94 | 0.83 | 1.93 | 1.81 | 1.28 | 725 | 450 |

^a Measured directly by disappearance of porphyrin S₁ state.

^b From steady-state fluorescence quenching data and fluorescence lifetime of porphyrin **6** methyl ester.

near the top of the Marcus curve, where rates are relatively insensitive to the thermodynamic driving force. However, CR is clearly occurring in the inverted region of the Marcus curve, as indicated by the fact that k_{CR} is slowest in the least polar solvent, toluene, and is highest in the most polar solvent, DMF. This is exactly the opposite of what would be expected if CR were occurring in the normal region of the Marcus curve. The value of Φ_{CS} is highest in *o*-dichlorobenzene.

The ET dynamics for dyads **9a** and **9b** are summarized in Table 3, along with fluorescence data for tetraphenylporphyrin methyl ester **8**. H₂P singlet excited state lifetimes, the inverse of the rates of charge separation, were measured in two different ways. The first column shows transient absorption data, following the rate of disappearance of singlet–singlet absorption of H₂P in the visible. The second set of lifetimes derives from measurements of the fluorescence lifetime of the H₂P standard, and determination of the extent of quenching in the dyads in three different solvents. The lifetime of the H₂P singlet excited state is then calculated by assuming that I/I_0 is equal to τ/τ_0 . Although the lifetimes determined by the two methods differ slightly, the trend is the same, namely k_{CS} increases with increasing solvent polarity, consistent with normal Marcus region behavior. The CR process, on the other hand, is clearly occurring in the Marcus inverted region, as the lifetime in THF far exceeds that in benzonitrile, a more polar solvent in which the CSRP state is lower in energy relative to the ground state than it is in THF. The very long lifetime of the CSRP state of **9b** in THF, namely 725 ns, is one of the longest ever measured for a simple P–C₆₀ dyad in solution.^{16,22}

3. Zinc porphyrin–fullerene dyads (ZnP–C₆₀)

3.1. Synthesis and structural characterization

Complexation of dyads **9a** and **9b** with zinc proceeded quantitatively using Zn(OAc)₂ in methanol, generating ZnP–C₆₀ **9aZn** and **9bZn**. Since zinc porphyrins are in general better electron donors than their free base counterparts, **9aZn** and **9bZn** were expected to generate CSRP states more rapidly and with a higher quantum yield than their free base analogs. Electronic ZnP–C₆₀ interactions in **9aZn** and **9bZn**, as monitored by UV–vis spectroscopy, are similar to those in **9a** and **9b**. Whereas red shifts in the absorption spectra were observed, the trend as a function of solvent polarity was not quite as clear as it was with the H₂P–C₆₀. An increase in solvent polarity increased the interaction, particularly in the dyad with

the longer linker, **9bZn**. Eventually, in the most polar solvents studied, the UV–vis spectra of ZnP–C₆₀ display nearly identical interactions to those in the H₂P–C₆₀ analogs. It is known that fullerene–porphyrin interactions are not as strong in metallated as in free base porphyrins, consistent with a larger distance between the chromophores in fullerene–metalloporphyrin co-crystals.⁹ Interchromophoric interactions prevail also in chelating solvents such as benzonitrile and THF, as clear shifts and bleaching in all absorption bands are observed upon comparison to the Zn-porphyrin standard.

3.2. Electrochemistry

For **9aZn**, the first oxidation (0.95 V) of the porphyrin center is shifted negatively by 150 mV and the reduction (–0.65 V) of C₆₀ is shifted negatively by 100 mV relative to appropriate standards. For **9bZn**, the first one-electron oxidation of the porphyrin center occurs at 0.92 V and the first one-electron reduction of the C₆₀ center appears at –0.59 V. There is a negative shift of 160 mV for the porphyrin center from **9b** to **9bZn**, consistent with the well known greater ease of oxidation of zinc versus free base porphyrins.

3.3. Steady-state fluorescence

Experiments for **9aZn** and **9bZn** were conducted using an excitation wavelength of 520 nm. The relative quenching efficiencies, relative to that of the ZnP standard, are similar to those observed in the corresponding H₂P–C₆₀. However, since the fluorescence lifetime of ZnP is typically on

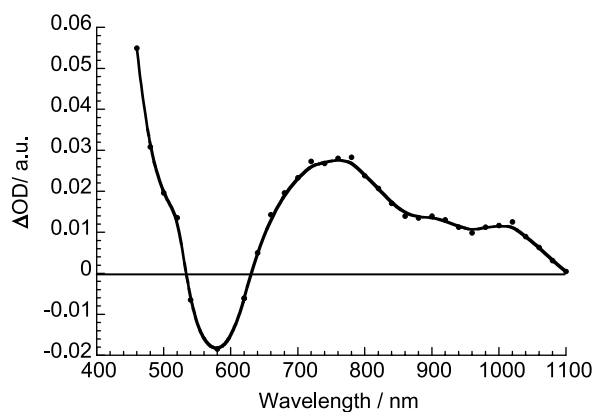


Figure 5. Differential absorption spectrum (visible and near-infrared) obtained upon nanosecond flash photolysis (532 nm) of $\sim 1.0 \times 10^{-5}$ M solutions of **9bZn** in nitrogen-saturated THF with a time delay of 50 ns at room temperature. The spectrum corresponds to the radical pair $ZnP^{+\cdot}-C_{60}^{\cdot-}$.

Table 4. Charge transfer dynamics for dyads **9aZn** and **9bZn**

| Compound | τ_F (ns) ^a | | | τ_{CS} (ns) | |
|-------------|----------------------------|------|------|------------------|------|
| | PhMe | THF | PhCN | THF | PhCN |
| 8Zn | 2.1 | 2.1 | 2.1 | | |
| 9aZn | 0.24 | 0.21 | 0.11 | 490 | 180 |
| 9bZn | 0.56 | 0.50 | 0.49 | 440 | 150 |

^a Measured by comparing steady-state fluorescence results to lifetime of Zn-porphyrin standard.

the order of ~ 2 ns, compared to 9 ns for the corresponding H_2P , the intramolecular CS rates in the $ZnP-C_{60}$ are clearly faster. As with the H_2P-C_{60} analogues, increased quenching with increasing solvent polarity is observed for the $ZnP-C_{60}$.

3.4. Transient absorption measurements

The fate of the ZnP singlet excited state in **9aZn** and **9bZn** was also examined by pico-, nano-, and microsecond transient absorption spectroscopies. At early times (i.e., 50–100 ps), these are practically identical to those of the $ZnTPP$, disclosing strong bleaching at 550 nm and attesting to the formation of the ZnP singlet excited state. At a delay time of ca. 200 ps, a new transition around 640 nm starts to grow in, accompanied by another absorption in the near-infrared. Based on a spectral comparison, we ascribe the former to the ZnP π -radical cation, while the latter band belongs to the C_{60} π -radical anion. The CSR absorption is persistent on the picosecond time scale and decays in the nano- to microsecond time regime (see Fig. 5).

The ET dynamics in several solvents are tabulated in Table 4. The rates of charge separation in **9aZn** and **9bZn** are consistently faster than those in **9a** and **9b**, by up to as much as an order of magnitude. This is hardly surprising since CS in the Zn -dyads is thermodynamically more favorable, which would lead to faster rates in an ET process occurring in the normal region of the Marcus curve. The charge recombination data again display inverted Marcus region behavior, as longer lifetimes are observed in THF than in benzonitrile.

4. Conclusions

The synthesis of a series of porphyrin- C_{60} dyads with flexible polyether linkers of varying length has been accomplished using a standard set of reactions. Introduction of alkyl substituents on the porphyrin greatly increased the solubility and ease of handling of these compounds. Using steady-state and time resolved techniques, it was found that the rate constants for forward electron transfer in both free base (H_2P) and ZnP systems, are on average approximately three orders of magnitude greater than the rate constants associated with back electron transfer. The formation of C_{60} triplet states in toluene for the free base dyads is attributed to ET followed by charge recombination, rather than a direct energy transfer mechanism, analogous to the situation in some other types of dyads. Fullerene triplets are not detected for the ZnP dyads in either polar or nonpolar solvents.

In these systems, the rapidity of the photoinduced ET process is best rationalized in terms of the molecular conformations of these dyads shown in Figure 1. It was reported by Armaroli et al.²⁴ that a doubly-linked face-to-face porphyrin-fullerene system and a related singly linked system show remarkably similar photophysical behavior, indicating that the donor and acceptor moieties in both these systems are in close proximity, and that through space rather than through-bond ET mechanisms dominate. On the other hand, there are some significant differences between the results of the present study and those reported for analogous doubly-linked dyads with parachute topology.¹³ The linkers in both cases are polyethers. The rates of charge separation in the present system are slightly slower than those in the parachute system by up to an order of magnitude, while the rates of charge recombination in the flexibly linked dyads are considerably slower, by closer to three orders of magnitude. For example, in THF the fluorescence lifetime of **5a** is 0.15 ns compared to 0.02–0.08 ns for the parachute dyad in the same solvent, while the CSR lifetime of **5a** is 300 ns, compared to 0.3 ns for the parachute compound. This difference can be rationalized in terms of significant differences in topology of the systems, but also suggests that through-bond ET processes may compete with through space mechanisms in the flexibly linked dyads, particularly with respect to charge recombination.

We conclude that the forward ET process in these flexibly linked donor-acceptor systems occurs near the peak of the Marcus parabola relating ET rates and thermodynamic driving force, while BET occurs deep in the inverted region, resulting in charge-separated radical pair (CSR) states with lifetimes approaching the microsecond time regime. This has obvious implications with respect to use of such systems in energy storage devices.²²

5. Experimental

All starting materials and solvents were purchased from Sigma-Aldrich and used without purification unless otherwise noted. ¹H NMR spectra were collected using a Gemini-200 MHz spectrometer. UV-vis spectra were collected using a Perkin-Elmer Lambda 35 UV-vis spectrometer. Fluorescence spectra were acquired using a Shimadzu RF-5301 PC fluorescence spectrophotometer. A gas chromatography mass spectrometer with an HP 5890 mass selective detector was used to acquire GC-MS data. MALDI-MS data were collected using an Omnicflex MALDI-TOF mass spectrometer. FAB-MS data were collected in collaboration with the Michigan State Mass Spectrometry Facility. HPLC was performed using a Milton-Roy 4000 obtained courtesy

of Prof. Ira Krull at Northeastern University. The HPLC column was a Buckyclutcher 1, using 15 μL injections. Fluorescence lifetime data was collected using a Pico-Quant Fluo-Time 100 time-resolved spectrophotometer. Pico-second laser flash photolysis experiments were carried out with 532 nm laser pulses from a mode-locked, Q-switched Quantel YG-501 DP Nd:YAG laser system (18 ps pulse width, 2–3 mJ/pulse). Nanosecond Laser Flash Photolysis experiments were performed with laser pulses from a Quanta-Ray CDR Nd:YAG system (532 nm, 6 ns pulse width) in a front face excitation geometry.

5.1. Modified synthesis of 3,5-di-*tert*-butylbenzaldehyde

A solution of 3,5-di-*tert*-butyltoluene (21.84 g, 107 mmol) and *N*-bromosuccinimide (26.66 g, 150 mmol) in benzene (55 mL) was heated at reflux under visible light irradiation. The reaction was then cooled, filtered, the benzene was removed under reduced pressure and the residue was added to a solution of hexamethylenetetramine (45.00 g, 321 mmol) in a 1:1 $\text{H}_2\text{O}/\text{EtOH}$ mixture (64 mL). The solution was heated at reflux for 4 h, concd HCl was added (21 mL) and heating at reflux was continued for 30 min. The ethanol was removed under reduced pressure, and the remaining aqueous layer was extracted with ether. The ether layer was dried (MgSO_4) and the solvent was removed under reduced pressure. Recrystallization from EtOH yielded the desired product as white crystals (66%).

5.1.1. 3,5-Di-*tert*-butylphenyl dipyrromethane 7.

A solution of the above aldehyde (3.581 g, 16.4 mmol) and freshly distilled pyrrole (28.4 mL, 409 mmol) was stirred under Ar at room temperature. Trifluoroacetic acid (0.13 mL, 16.4 mmol) was added dropwise, and the solution was stirred an additional 30 min. An excess of triethylamine (0.3 mL) was added to quench the reaction, and the pyrrole was removed under reduced pressure. The crude product was dissolved in CH_2Cl_2 and extracted with 0.1 M aqueous NaOH and water, dried (Na_2SO_4) and the solvent was removed under reduced pressure. Flash chromatography yielded the dipyrromethane derivative as a sticky light brown solid (51%) (SiO_2 , 85:14:1 Cyclohexane/EtOAc/ Et_3N , $R_f=0.5$). The material was characterized by its 200 MHz ^1H NMR spectrum, 50 MHz ^{13}C NMR spectrum and GC/MS analysis.²³

5.1.2. 5-(4'-Carboxymethylphenyl)-10,15,20-tris-(3,5-di-*tert*-butyl-phenyl)porphyrin 6. A solution of dipyrromethane **6** (3.00 g, 9.0 mmol), 3,5-di-*tert*-butylbenzaldehyde (0.979 g, 4.5 mmol), and 4-carboxymethyl benzaldehyde (0.736 g, 4.5 mmol) in dry CH_2Cl_2 (900 mL) was stirred at room temperature under Ar. Trifluoroacetic acid (0.69 mL, 16 mmol) was added dropwise and the mixture was stirred an additional 1 h. Excess 2,3-dichloro-5,6-dicyano-1,4-benzoquinone (DDQ) (3 g) was added and the solution was stirred open to the air for an additional 2 h. The solvent was removed under reduced pressure and the product was purified via flash chromatography (17%) (6:4 Hexanes/EtOAc, $R_f=0.5$). The porphyrin ester **8** was characterized by ^1H NMR and MALDI-MS analysis.²³

A solution of **8** (250 mg) in isopropanol was heated at reflux. A solution of KOH (1.4 g) in water (12.5 mL)

was added dropwise, and the solution was heated at reflux for 6 h. The solvent was removed under reduced pressure, the residue was dissolved in CH_2Cl_2 and then extracted sequentially with 1 M HCl and water. After drying over Na_2SO_4 , the solvent was removed under reduced pressure, and the final porphyrin carboxylic acid **6** was purified via flash chromatography (yield 94%) (SiO_2 , 1:9 MeOH/ CH_2Cl_2 , $R_f=0.5$). The material was characterized by ^1H NMR and MALDI-MS analysis.²³

5.1.3. Glycol-C₆₀ adducts 3a and 3b. General procedure: bromobenzene was added to an Ar-purged flask containing fullerene carboxylic acid **1** (1 equiv), DMAP (0.2 equiv), 1-hydroxybenzotriazole hydrate (1.1 equiv) and dicyclohexylcarbodiimide (DCC) (10 equiv). The appropriate diol (10 equiv) was added in DMSO, and the reaction was held at 50 °C with stirring for 18 h. Bromobenzene was removed under reduced pressure and the crude product was dissolved in CH_2Cl_2 and extracted sequentially with water, 10% aqueous CaSO_4 and brine. The final solution was dried (Na_2SO_4) and the solvent was removed under reduced pressure. The residue was purified by flash chromatography (SiO_2 , 10% EtOAc/PhMe) to give **3a** (61%) and **3b** (64%), respectively.

5.1.4. Synthesis of dyads 9a and 9b. General procedure for EDC/DMAP coupling: to a solution of porphyrin acid **6** (1.01 equiv), EDC (1.01 equiv) and DMAP (1.01 equiv) in the minimum amount of dry CH_2Cl_2 , a solution of C₆₀ carboxylic acid derivative **3a** or **3b** (1 equiv) in CH_2Cl_2 was added at room temperature. The mixture was stirred for 18 h, diluted with CH_2Cl_2 (20 mL), washed with a solution of saturated aqueous NH_4Cl (3 \times 20 mL) and brine (2 \times 20 mL), dried (Na_2SO_4) and finally evaporated to give the crude dyad, which was purified via flash chromatography to give the pure material. Dyad **9a**: 51% (10% EtOAc/PhMe, $R_f=0.25$); Dyad **9b**: 47% (10% EtOAc/PhMe, $R_f=0.2$). The final products were characterized by ^1H NMR and MALDI-MS analysis.²³

5.2. Singlet molecular oxygen emission measurements

These experiments were done following the procedure described in a previous paper in this series.¹³

Acknowledgements

D.I.S. and S.M. are grateful to the US National Science Foundation for support of their work at NYU, under grant CHE-009789. L.E. also gratefully acknowledges NSF support for the work at Clemson.

References and notes

- (a) Imahori, H.; Sakata, Y. *Adv. Mater.* **1997**, *9*, 537. (b) Prato, M. *J. Mater. Chem.* **1997**, *7*, 1097. (c) Martin, N.; Sánchez, L.; Illescas, B.; Pérez, I. *Chem. Rev.* **1998**, *98*, 2527. (d) Imahori, H.; Sakata, Y. *Eur. J. Org. Chem.* **1999**, 2445. (e) Diederich, F.; Gómez-López, M. *Chem. Soc. Rev.* **1999**, *28*, 263. (f) Guldi, D. M. *Chem. Commun.* **2000**, 321. (g) Reed, C. A.; Bolskar, R. D. *Chem. Rev.* **2000**, *100*, 1075. (h) Gust, D.;

- Moore, T. A.; Moore, A. L. *J. Photochem. Photobiol., B* **2000**, *58*, 63. (i) Gust, D.; Moore, T. A.; Moore, A. L. *Acc. Chem. Res.* **2001**, *34*, 40. (j) Guldi, D. M.; Martin, N. *J. Mater. Chem.* **2002**, *12*, 1978–1992. (k) Guldi, D. M. *Chem. Soc. Rev.* **2002**, *31*, 22. (l) Imahori, H.; Mori, Y.; Matano, Y. *J. Photochem. Photobiol., C* **2003**, *4*, 51. (m) Nierengarten, J. F. *Top. Curr. Chem.* **2003**, *228*, 87. (n) Guldi, D. M. *Pure Appl. Chem.* **2003**, *75*, 1069. (o) El-Khouly, M. E.; Ito, O.; D'Souza, F. *J. Photochem. Photobiol., C* **2004**, *5*, 79. (p) Guldi, D. M.; Prato, M. *Chem. Commun.* **2004**, 2517.
2. Xie, Q.; Perez-Cordero, E.; Echegoyen, L. *J. Am. Chem. Soc.* **1992**, *114*, 3978.
3. Imahori, H.; Hagiwara, K.; Akiyama, T.; Aoki, M.; Taniguchi, S.; Okada, T.; Shirakawa, M.; Sakata, Y. *Chem. Phys. Lett.* **1996**, *263*, 545.
4. (a) Guldi, D. M.; Luo, C.; Prato, M.; Dietel, E.; Hirsch, A. *Chem. Commun.* **2000**, 373. (b) Imahori, H.; Tamaki, K.; Guldi, D. M.; Luo, C.; Fujitsuka, M.; Fukuzumi, S. *J. Am. Chem. Soc.* **2001**, *123*, 2607. (c) Imahori, H.; Yamada, H.; Guldi, D. M.; Endo, Y.; Shimomura, A.; Kundu, S.; Yamada, K.; Okada, T.; Sakata, Y.; Fukuzumi, S. *Angew. Chem., Int. Ed.* **2002**, *41*, 2344. (d) Ohkubo, K.; Imahori, H.; Shao, J. G.; Ou, Z. P.; Kadish, K. M.; Chen, Y. H.; Zheng, G.; Pandey, R. K.; Fujitsuka, M.; Ito, O.; Fukuzumi, S. *J. Phys. Chem. A* **2002**, *106*, 10991. (e) Fukuzumi, S.; Ohkubo, K.; Imahori, H.; Guldi, D. M. *Chem. Eur. J.* **2003**, *9*, 1585.
5. (a) Lindsey, J. S.; Schreiman, I. C.; Hsu, H. C.; Kearney, P. C.; Marguerettaz, A. M. *J. Org. Chem.* **1987**, *52*, 827. (b) Lee, C. H.; Lindsey, J. S. *Tetrahedron* **1994**, *50*, 11427. (c) Littler, B. J.; Ciringh, Y.; Lindsey, J. S. *J. Org. Chem.* **1999**, *64*, 2864. (d) Smith, K. M. *J. Porphyrins Phthalocyanines* **2000**, *4*, 319.
6. Boyd, P. D. W.; Hodgson, M. C.; Rickard, C. E. F.; Oliver, A. G.; Brothers, P. J.; Chaker, L.; Bolskar, R. D.; Tham, F. S.; Reed, C. A. *J. Am. Chem. Soc.* **1999**, *121*, 10487.
7. Imahori, H.; Guldi, D. M.; Tamaki, K.; Yoshida, Y.; Luo, C.; Sakata, Y.; Fukuzumi, S. *J. Am. Chem. Soc.* **2001**, *123*, 6617.
8. Baran, P. S.; Monaco, R. R.; Khan, A. U.; Schuster, D. I.; Wilson, S. R. *J. Am. Chem. Soc.* **1997**, *119*, 8363. Schuster, D. I. *Carbon* **2000**, *38*, 1607.
9. Nierengarten, J.-F.; Herrmann, A.; Tykwinski, R. R.; Ruttimann, M.; Diederich, F.; Boudon, C.; Gisselbrecht, J. P.; Gross, M. *Helv. Chim. Acta* **1997**, *80*, 293.
10. (a) MacMahon, S.; Wilson, S. R.; Schuster, D. I. *Proc. Electrochem. Soc.* **2000**, *8*, 155. (b) MacMahon, S.; Fong, R.; Baran, P. S.; Safonov, I.; Wilson, S. R.; Schuster, D. I. *J. Org. Chem.* **2001**, *66*, 5449.
11. Schuster, D. I.; Jarowski, P. D.; Kirschner, A. N.; Wilson, S. R. *J. Mater. Chem.* **2002**, *12*, 2041.
12. Bourgeois, J.-P.; Diederich, F.; Echegoyen, L.; Nierengarten, J.-F. *Helv. Chim. Acta* **1998**, *81*, 1835.
13. Schuster, D. I.; Cheng, P.; Jarowski, P. D.; Guldi, D. M.; Luo, C.; Echegoyen, L.; Pyo, S.; Holzwarth, A. R.; Braslavsky, S. E.; Williams, R. M.; Klihm, G. *J. Am. Chem. Soc.* **2004**, *126*, 7257.
14. Ogilby, P. R.; Foote, C. S. *J. Am. Chem. Soc.* **1982**, *104*, 2069.
15. Arbogast, J. W.; Darmanyan, A. P.; Foote, C. S.; Rubin, Y.; Diederich, F. N.; Alvarez, M. M.; Anz, S. J.; Whetten, R. L. *J. Phys. Chem.* **1991**, *95*, 11. Bensasson, R. V.; Bienvenue, E.; Dellinger, M.; Leach, S.; Seta, P. *J. Phys. Chem.* **1994**, *98*, 3492.
16. For a review, see: Bracher, P. J.; Schuster, D. I. In *Fullerenes: From Synthesis to Optoelectronic Properties*; Guldi, D. M., Martin, N., Eds.; Kluwer Academic: Dordrecht, 2002; pp 163–212.
17. Kuciauskas, D.; Lin, S.; Seely, G. R.; Moore, A. L.; Moore, T. A.; Gust, D.; Drovetskaya, T.; Reed, C. A.; Boyd, P. D. W. *J. Phys. Chem.* **1996**, *100*, 15926–15932.
18. Galili, T.; Regev, A.; Levanon, H.; Schuster, D. I.; Guldi, D. M. *J. Phys. Chem. A* **2004**, *108*, 10632–10639.
19. Armaroli, N.; Accorsi, G.; Felder, D.; Nierengarten, J.-F. *Chem. Eur. J.* **2002**, *8*, 2314–2323.
20. Guldi, D. M.; Prato, M. *Acc. Chem. Res.* **2000**, *33*, 695.
21. (a) Guldi, D. M.; Luo, C.; Da Ros, T.; Prato, M.; Dietel, E.; Hirsch, A. *Chem. Commun.* **2000**, 375. (b) Luo, C.; Guldi, D. M.; Imahori, H.; Tamaki, K.; Sakata, Y. *J. Am. Chem. Soc.* **2000**, *122*, 6535. (c) Guldi, D. M.; Luo, C.; Prato, M.; Dietel, E.; Hirsch, A. *Chem. Commun.* **2000**, 373. (d) Imahori, H.; Tamaki, K.; Guldi, D. M.; Luo, C.; Fujitsuka, M.; Ito, O.; Sakata, Y.; Fukuzumi, S. *J. Am. Chem. Soc.* **2001**, *123*, 2607. (e) Imahori, H.; Guldi, D. M.; Tamaki, K.; Yoshida, Y.; Luo, C.; Sakata, Y.; Fukuzumi, S. *J. Am. Chem. Soc.* **2001**, *123*, 6617. (f) Imahori, H.; Yamada, H.; Guldi, D. M.; Endo, Y.; Shimomura, A.; Kundu, S.; Yamada, K.; Okada, T.; Sakata, Y.; Fukuzumi, S. *Angew. Chem., Int. Ed.* **2002**, *41*, 2344. (g) Guldi, D. M.; Scheloske, M.; Dietel, E.; Hirsch, A.; Troisi, A.; Zerbetto, F.; Prato, M. *Chem. Eur. J.* **2003**, *9*, 4968. (h) Balbinot, D.; Atalick, S.; Guldi, D. M.; Hatzimarinaki, M.; Hirsch, A.; Jux, N. *J. Phys. Chem.* **2003**, *107*, 13273.
22. Guldi, D. M. *Chem. Soc. Rev.* **2002**, *31*, 22.
23. For details, see: MacMahon, S. Ph.D. Dissertation, New York University, 2004.
24. Armaroli, N.; Marconk, G.; Echegoyen, L.; Bourgeois, J.-P.; Diederich, F. *Chem. Eur. J.* **2000**, *6*, 1629–1645.